ChemSusChem

Chemistry–Sustainability–Energy–Materials

Chemistry Europe

European Chemical Societies Publishing

Accepted Article

Title: Joule-Heating-Driven Encapsulation of FeCo Nanoparticles in Ion-Selective Carbon Shell for Stable Seawater Electrolysis

Authors: Guanhao Kuang, Keyu Wang, Yixing Wang, Linfeng Lei, Linzhou Zhuang, and Zhi Xu

To be cited as: *ChemSusChem* **2025**, e202402710

Link to VoR: https://doi.org/10.1002/cssc.202402710

WILEY VCH

10.1002/cssc.202402710

Joule-Heating-Driven Encapsulation of FeCo Nanoparticles in Ion-Selective Carbon Shell for Stable Seawater Electrolysis

Guanhao Kuang,[a] Keyu Wang, [a] Yixing Wang,[a,b] Linfeng Lei,[a,b] Linzhou Zhuang,*[a] Zhi Xu*[a]

[a] State Key Laboratory of Chemical Engineering, East China University of Science and Technology, Shanghai, 200237, China

[b] Suzhou Laboratory, Suzhou, 215000, China

* Corresponding author: Zhi Xu (zhixu@ecust.edu.cn), Linzhou Zhuang (lzzhuang@ecust.edu.cn)

Abstract

The oxygen evolution reaction (OER) in seawater is notoriously hindered by slow kinetics and high overpotential, compounded by chloride-induced corrosion, which impedes efficient hydrogen production via seawater electrolysis. A key challenge is to devise an OER catalyst that not only mitigates chlorine oxidation and corrosion but is also cost-effective. In this work, the bimetallic iron-cobalt (FeCo) nanoparticles are swiftly encapsulated within N-doped carbon shells in mere seconds using the Joule-heating technique, a process significantly faster than the several hours required by traditional furnace heating. Meanwhile, the high temperature could offer the necessary activation energy for Fe/Co atom redispersion on the carbon shell via forming abundant metal-nitrogen (Co/Fe-N-C) active sites. These Co/Fe-N-C sites exhibit exceptional activity for OER catalysis. Consequently, the sample prepared by Joule-heating at 800 °C for 5 seconds (FeCo@CN-J-5) demonstrates superior OER performance, achieving a current density that is 35 times greater than that prepared without N doping and 6 times higher than that prepared via furnace heating. Moreover, FeCo@CN-J-5 operates stably for 100 hours at 200 mA cm^{-2} with negligible degradation in the highly corrosive electrolyte of 0.1 M KOH + 0.6 M NaCl, demonstrating its promising potential for practical seawater splitting.

Keywords: Joule heating, encapsulation, seawater splitting, ion selectivity, oxygen evolution

Introduction

The growing global economy is fueling a significant increase in energy demand, which relies heavily on fossil fuels and contributes to increased global environmental problems.[1-3] Hydrogen, as a clean energy source with high energy density and eco-friendliness, has attracted significant attention,[4-6] and electrochemical water splitting is considered one of the most ideal methods for hydrogen production.[7-10] While current research predominantly focuses on pure water electrolysis, seawater electrolysis holds great promise as a cost-effective, sustainable, and eco-friendly alternative for green hydrogen generation.[11-16] Direct seawater electrolysis poses greater challenges than pure water electrolysis due to the abundance of Cl^- ions, which can corrode catalysts and trigger competing side reactions.[17-20] The chlorine oxidation reaction (COR), which occurs due to the presence of Cl^- in seawater, competes with the OER on the anode and reduces the OER efficiency.[21-23] Therefore, it is crucial to develop OER catalysts with high catalytic activity, high selectivity, and excellent stability in direct seawater electrolysis.

Considering the kinetics and standard potentials, selective OER in alkaline seawater electrolysis is more suitable because it helps to inhibit chlorine generation in alkaline environments.[23-25] To develop efficient OER electrocatalysts under high-salinity conditions (~0.6 M NaCl) and low-alkalinity electrolytes, researchers have explored various strategies. For instance, Loomba et al. designed and prepared porous nitrogen-doped $NiMo_3P$ (N-$NiMo_3P$) nanosheets with a thickness of several micrometer size, whose abundant active sites and metal-nitrogen bonding was crucial for overcoming harsh seawater environments.[26] Kuang et al. found that the in situ generated sulfate- and carbonate-rich negative charge layers on the NiFe layered double hydroxide (LDH) catalyst could selectively repel Cl^- ions through electrostatic repulsive forces. This mechanism helped prevent corrosion of the inner catalytic species.[25] Luo et al. reported a three-dimensional (3D) core-shell TMN-based OER electrocatalyst with multi-scale porosity (NiMoN@NiFeN), which provided abundant active sites, facilitated rapid gaseous product release through interconnected channels, and enabled efficient charge

transfer, leading to excellent alkaline seawater splitting activity.[17] Moreover, the formation of a negatively charged layer on the catalyst could selectively repel Cl^-, which improved stability, but unfortunately, its catalytic activity could hardly be improved simultaneously.[27] Despite significant advances in OER catalysts for the seawater electrolysis have been achieved, there are still some challenges in enhancing the performance and stability of the catalysts. While FeCo-based catalysts demonstrate excellent electrocatalytic activity for the oxygen evolution reaction (OER), their chloride resistance and oxidation stability in seawater environments remain underexplored.[9, 28-32] Additionally, using conventional methods to control the formation of carbon shells typically required high temperatures (~800 °C) and longer durations (>2 h), leading to high energy consumption and extended processing times.

In this work, we achieved the transient construction of carbon shell on FeCo bimetallic core (FeCo@CN-J-5) via a Joule-heating technique that could minimize energy and time consumption. The transient high temperature could provide sufficient activation energy to enable the diffusion of Fe/Co atoms from the metal alloy core towards the exterior, and then these atoms could be captured by N-C anchoring sites. The formed Co/Fe-N-C coordination sites exhibited high OER catalytic activity and selectivity, and proper extension of the heating time led to the full redispersion of Fe/Co atoms in the N-doped carbon shell. Meanwhile, the carbon shell could well protect the metal core from corrosion. Thanks to this unique structure, the FeCo@CN-J-5 catalyst required a low overpotential of 299 mV to achieve the current density of 10.0 mA cm^{-2} in the electrolyte of 0.1 M KOH + 0.6 M NaCl, and could stably operate for over 100 hours at a high current density of 200 mA cm^{-2}.

Experimental section

Materials and chemicals

Cobalt chloride hexahydrate ($CoCl_2 \cdot 6H_2O$, 98%) and sodium chloride (NaCl, 99.8%) were purchased from Shanghai Aladdin Biochemical Technology Co., Ltd. Iron(III) chloride ($FeCl_3$, 99%)

was purchased from Shanghai Titan Scientific Co., Ltd. Potassium hydroxide (KOH, 95 %) and 2-methylimidazole ($C_4H_6N_2$) were purchased from MACKLIN. The SCP130N hydrophilic carbon paper was purchased from Suzhou Sinero Technology Co., Ltd, whose main parameters include thickness (0.3 mm), volume density (770 mg cm^{-3}), void ratio (75%), air resistance (11.5 mmH_2O), and electrical resistivity (through plane, 2.7 mΩ cm^2). All the chemicals and reagents were used without further purification.

Preparation of FeCo@CN-J-5

The FeCo@CN-J-5 was synthesized by rapid Joule-heating technique. Typically, 0.119 g of $CoCl_2 \cdot 6H_2O$ and 0.081 g of $FeCl_3$ were dissolved in 50 mL of deionized water under stirring for 10 minutes at room temperature. Separately, 0.68 g of 2-methylimidazole was dissolved in another 50 mL of deionized water. Then the Fe and Co precursor solution and 2-methylimidazole solution were dropped on a 1×1.5 cm^2 carbon paper (SCP130N) in batches, and rapidly dried (~65ºC) by infrared heating lamp. After drying, it was placed in the middle of two 3 × 6 cm^2 carbon paper (SCP130N) to form a sandwich structure to ensure uniform heating of the sample, and thermally treated by applying high voltage and high current to generate Joule-heating in a glovebox filled with an argon atmosphere. The voltage and current were set to 30 V and 38.5 A, respectively, and the power-on time could be 1 s, 2 s, 3 s, 4 s, and 5 s (FeCo@CN-J-X). The surface temperature of the carbon paper was about 800 ℃. FeCo@CN-J-X samples were then collected for subsequent activity evaluation.

Preparation of FeCo@C-J-5

To reveal the effect of N doping on the diffusion of metal atoms during Joule-heating treatment, the FeCo@C-J-5 sample (without N doping) was prepared, whose synthesis method was similar to that of

FeCo@CN-J-5, except that no 2-methylimidazole was added, and the solution added by drops was only the Fe/Co precursor mixture solution.

Preparation of FeCo@CN-T-800-2

To reveal the differences between Joule-heating treatment and tubular furnace heating methods, the FeCo@CN-T-800-2 sample was prepared. The Fe/Co mixture solution and 2-methylimidazole solution were dropped on a 1 × 1.5 cm^2 carbon paper (SCP130N) in batches, infrared heating (~ 65 ℃) by an infrared heating lamp caused the solution to volatilize rapidly. After drying, the sample was placed in a porcelain boat and heated to 800 ℃ at a rate of 5 ℃ min^{-1} in flowing argon atmosphere for 2 h.

Results and discussion

Preparation and morphological characterization

The preparation procedure of FeCo@CN-J-5 via rapid Joule-heating technique is shown in Figure 1a and illustrated in the Experimental Section.[9] The morphology of FeCo@C-J-5 and FeCo@CN-J-5 were first characterized by transmission electron microscopy (TEM). As shown in Figure 1b and Figure S1, the carbon layer of FeCo@C-J-5 incompletely encapsulated the FeCo metal nanoparticles in the absence of nitrogen doping. In contrast, after nitrogen doping, a well-defined carbon shell formed, effectively encapsulating the metal nanoparticles (Figure 1c). X-ray diffraction (XRD) was then used to characterize the crystal structure and composition of the catalysts (Figure 1d and Figure S2). FeCo@CN-J-5 exhibited two diffraction peaks representing FeCo metal alloy at 44.750º and 65.108º (PDF#48-1816), and their intensities were higher than that of FeCo@C-J-5. Meanwhile, the results of inductively coupled plasma (ICP-OES) showed that the Fe and Co contents of FeCo@CN-J-5 were more than two times that of FeCo@C-J-5 (Table S1). Moreover, X-ray photoelectron spectroscopy

(XPS) was used to investigate the surface chemical composition and electronic structure of FeCo@CN-J-5 and FeCo@C-J-5. Figure S3 and Figure S4 showed the survey-scan XPS spectra of FeCo@CN-J-5 and FeCo@C-J-5, while the surface contents of Co, Fe, and N elements obtained from the XPS survey spectra (Figure S3 and Figure S4) were listed in Table S2, showing that the contents of Co and Fe elements were significantly increased after N doping. XPS results, together with XRD and ICP results, fully proved that the existence of N species was crucial for enhancing the adsorption capacity of Fe/Co atoms on the carbon shell matrix, thus increasing the loading content of FeCo metal nanoparticles.

Specifically, the N 1s spectra (Figure 1e) could be deconvoluted into pyridinic N (398.6 eV), porphyrin-like M-N_x coordination (399.8 eV), and pyrrolic N (401.5 eV), indicating the successful introduction of abundant N atoms into the carbon matrix.[33] It has been reported that the lone pairs of electrons or electron clouds on pyridine N could interact with the π-electron system of neighboring carbon atoms, thus changing the electron density distribution of the carbon atoms to enhance the oxygen adsorption and reduction processes.[34] Pyridine N could also be promising anchoring sites for Fe and Co atoms to exhibit excellent catalytic performance and electron conductivity.[35] Figure S5 confirmed the existence of metal-O coordination.[36] Thus, the Co 2p spectra of FeCo@C-J-5 and FeCo@CN-J-5 were collected and depicted in Figure 1f. The peak of Co $2p_{3/2}$ could be deconvoluted into three peaks centering at around 780.4, 782.9, and 787.6 eV, attributed to Co^{3+}, Co^{2+}, and satellite, respectively. For the Fe 2p spectra (Figure 1g), and the binding energy at 714.2 eV confirmed the presence of Fe^{3+}, while the peak located at about 711.2 eV could be attributed to Fe^{2+}. The presence of Fe^{2+} and Co^{3+} could be attributed to the charge transfer that occurred between Fe and Co species during Joule-heating. To summarize, TEM and XPS results showed that C, N, O, Fe and Co were all presented in FeCo@CN-J-5, and the synthesized FeCo@CN-J-5 was encapsulated by amorphous N-doped carbon shells with Co/Fe-N-C coordination sites.

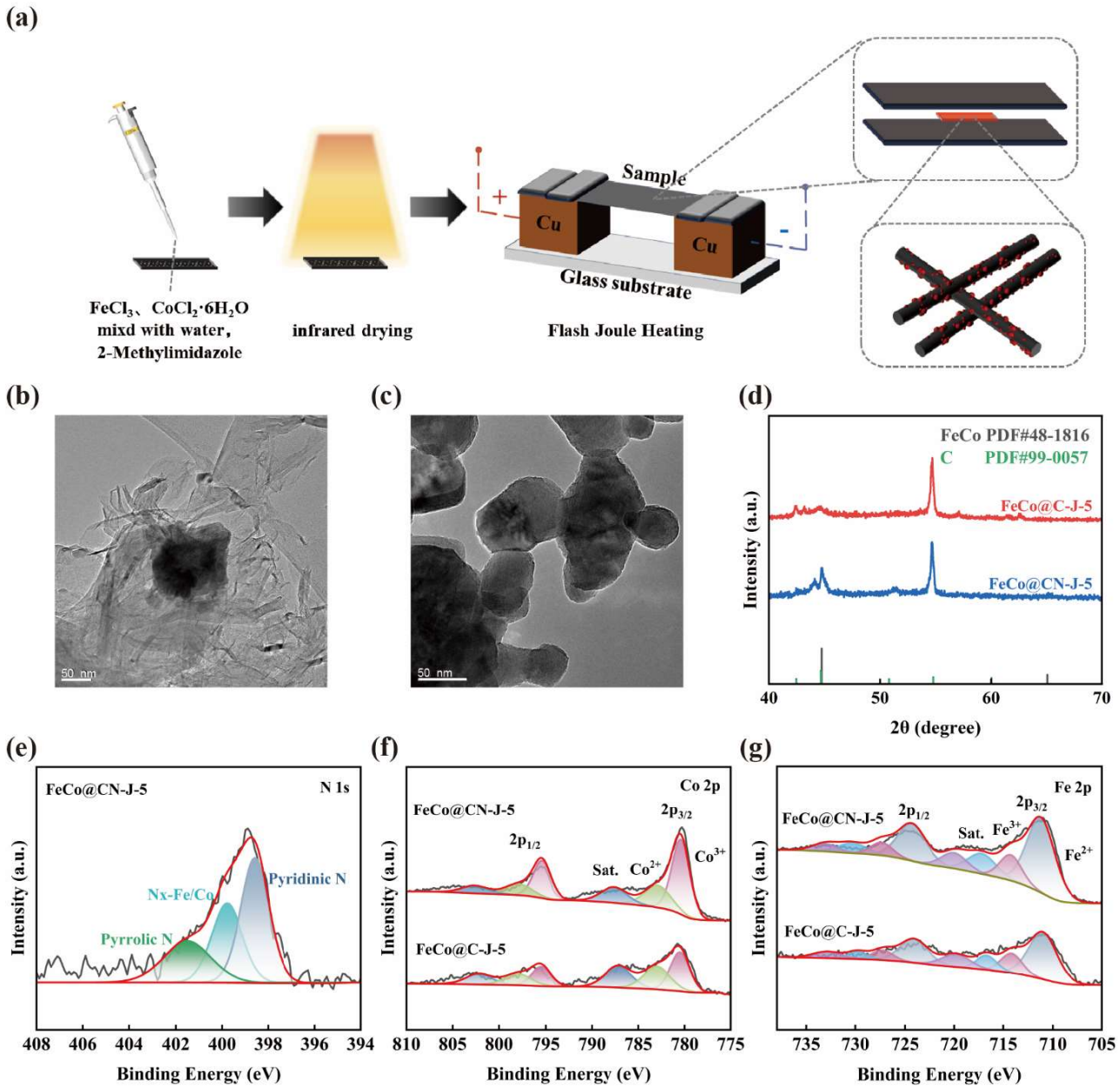

Figure 1. The synthesis route and morphological characterization. (a) A schematic illustration of the synthesis process of FeCo@CN-J-5. (b) TEM image of FeCo@C-J-5. (c) TEM image of FeCo@CN-J-5. (d) The XRD pattern of FeCo@C-J-5, FeCo@CN-J-5. (e-g) XPS spectra of FeCo@C-J-5, FeCo@CN-J-5.

Structure evolution under Joule heating

TEM was further employed to compare the FeCo@CN-J-1 and FeCo@CN-J-5 samples with those prepared under different heating durations. The FeCo@CN-J-1 sample exhibited a well-defined carbon shell surrounding the metal nanoparticles (Figure 2a and Figure S6), and under TEM observation, the carbon shell appeared transparent as it could be penetrated by electrons. As the heating duration increased, Fe/Co atoms of the metal core could diffuse outwards and be captured by the N anchoring sites within carbon shell, which became impervious to the electron penetration under TEM observation. Consequently, the thickness of the transparent carbon out layer progressively decreased from 8.4 nm to 3.3 nm when the Joule-heating duration increased from 1 s to 4 s. Eventually, in FeCo@CN-J-5, the Fe/Co atoms were homogeneously dispersed throughout the N-doped carbon shell, and the nanoparticle sizes were primarily distributed within the range of 45-80 nm, with the majority of nanoparticles centered around 50 nm (Figure 2a-e and Figure S7). The EDS spectrum of FeCo@CN-J-5 is shown in Figure 2f, confirming that the C, N, O, Fe, and Co elements were dispersed in the core-shell structure, proving the formation of Co/Fe-N_4-C coordination sites, which were expected to enhance the OER activity of the catalysts. Based on the above results, the dispersion process of the Fe/Co atoms from the metallic alloy core into the N-doped carbon shell during Joule-heating could be clearly illustrated (as shown in Figure 2g). High-temperature Joule heating provides sufficient activation energy for atomic diffusion, and initially, as the inner carbon layer contained abundant N sites, the diffused Fe/Co atoms could be preferentially captured by the N sites of inner carbon layer to form the Fe/Co-N-C coordination. However, once the N sites of inner carbon layer were occupied and in short supply, Fe/Co atoms continued to diffuse outwards, eventually achieving complete dispersion of the atoms into throughout carbon shell. In other words, this results in the formation of more active sites, which is more beneficial for the OER to proceed. [37]

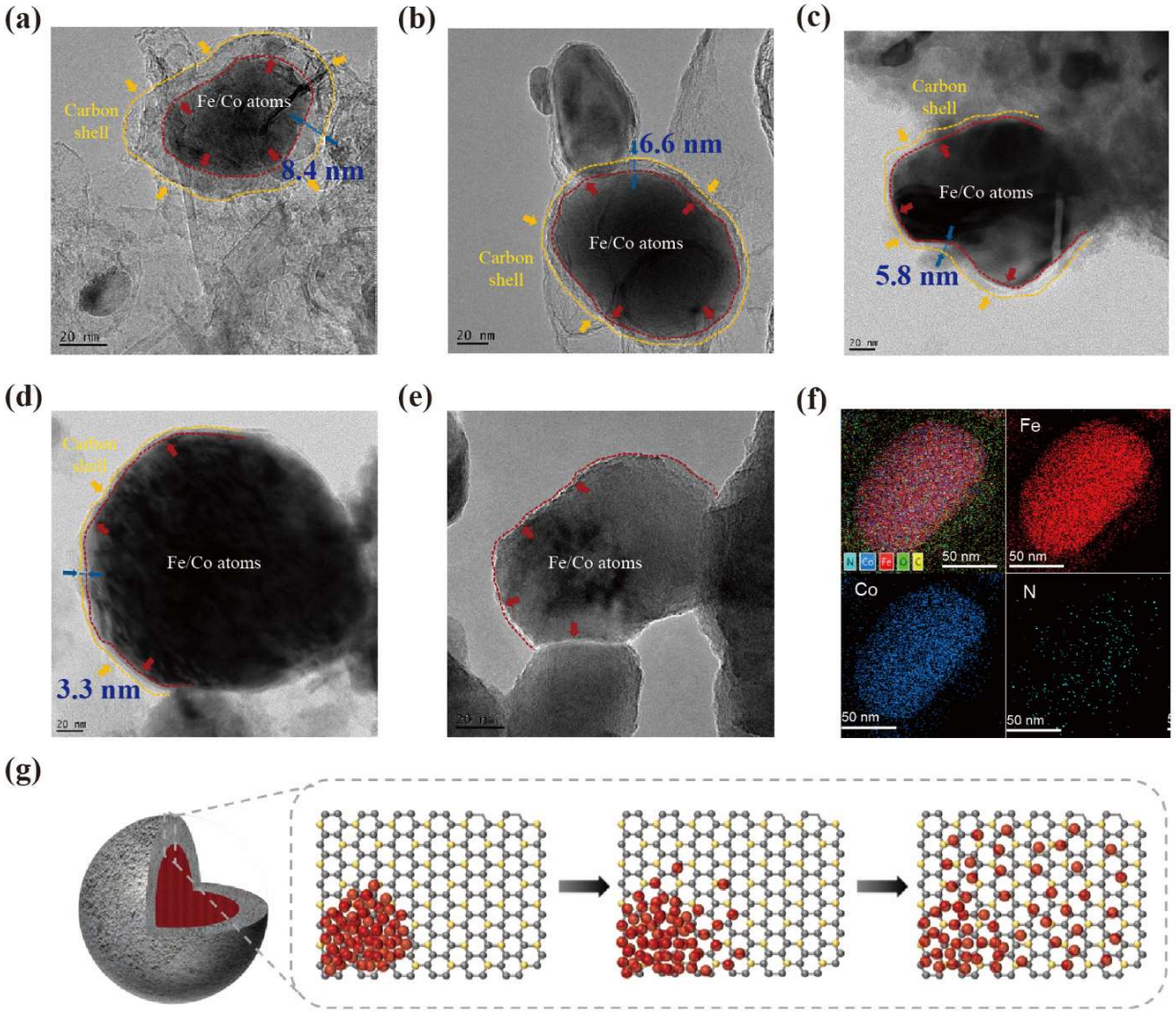

Figure 2. The Structural changes of FeCo@CN-J-X after different Joule heating times. (a-e) TEM images of FeCo@CN-J-1, FeCo@CN-J-2, FeCo@CN-J-3, FeCo@CN-J-4, FeCo@CN-J-5. (f) HAADF STEM image and EDX elemental maps of FeCo@CN-J-5. (g) A schematic illustration of the evolution of the carbon shell structure.

Electrochemical activity evaluation

The OER activities of FeCo@C-J-5, FeCo@CN-J-X (X=1,3,5,8,10) were evaluated using a three-electrode system in 0.1 M KOH + 0.6 M NaCl solution and 1M KOH solution at a scanning rate of 1 mV s^{-1} at room temperature (Figure S8-9). As shown in Figure 3a and Figure S10, FeCo@CN-J-5 had

the lowest overpotential value of 299 mV at a current density of 10 mA cm^{-2}, followed by FeCo@CN-J-1 at 317 mV, both of which were far superior to FeCo@C-J-5 without N-doping (394 mV). Meanwhile, at the overpotential of 350 mV, the current density of FeCo@CN-J-5 (125 mA cm^{-2}) was 35 times that of FeCo@C-J-5 (3.8 mA cm^{-2}). We further investigated the Tafel slope of the catalysts, which could be applied to determine the reaction kinetics of the catalysts (Figure 3b). Compared with the Tafel slopes of FeCo@C-J-5 (71.9 mV dec^{-1}) and FeCo@CN-J-1 (58.7 mV dec^{-1}), the Tafel slope of FeCo@CN-J-5 was smaller (44.7 mV dec^{-1}), suggesting the enhanced OER kinetics of FeCo@CN-J-5. Meanwhile, the charge transfer of the prepared catalysts in alkaline seawater was analyzed by electrochemical impedance spectroscopy (EIS) at a voltage of 1.56 V (vs. RHE), and the Nyquist plots were illustrated in Figure 3c. The R_{ct} value of FeCo@CN-J-5 was 7.6 Ω, smaller than that of FeCo@CN-J-1 (10.0 Ω) and FeCo@C-J-5 (18.5 Ω), which suggested that FeCo@CN-J-5 possessed the optimal electron transfer capability. The electrochemical active surface area (ECSA) of the catalyst was positively correlated with its double layer capacitance (C_{dl}), which was measured by cyclic voltammetry and scanned at different scanning rates (20 mV s^{-1} to 100 mV s^{-1}) (Figure S11). As shown in Figure 3d, the C_{dl} value of FeCo@CN-J-5 (34.9 mF cm^{-2}) was much larger than that of FeCo@CN-J-1 (27.4 mF cm^{-2}) and FeCo@C-J-5 (11.7 mF cm^{-2}). Accordingly, the ECSA values of FeCo@C-J-5, FeCo@CN-J-1, and FeCo@CN-J-5 were 292.5 cm^2, 685 cm^2, and 872.5 cm^2, respectively. It could be seen that catalysts with N-doped carbon shell and metal particles distributed in the carbon shell had more active sites and good charge transfer properties, which significantly improved the OER performance. Clearly, FeCo@CN-J-5 exhibited the lowest overpotential and Tafel slope, as well as enhanced OER kinetics and electron transfer capability, which is advantageous for its application as OER catalyst. The intrinsic activity of FeCo@CN-J-5 indeed outperformed most recently reported transition metal catalysts in alkaline seawater (Table S5).

Stability was a key indicator for evaluating the catalytic performance of a sample. We compared the stability of FeCo@C-J-5 and FeCo@CN-J-5 in alkaline seawater splitting (0.1 M + 0.6 M NaCl).

Figure 3e showed the long-term stability of FeCo@C-J-5 and FeCo@CN-J-5 at the current density of 100 mA cm^{-2}. It could be seen that FeCo@C-J-5 started to decay in 40 h, and was completely deactivated after 80 h, while FeCo@CN-J-5 could operate stably at a current density of 100 mA cm^{-2} for over 100 h with negligible decay. It was clear from Figure S12 that the CV curve obtained after 100 h of operation at a current density of 100 mA cm^{-2} almost overlapped with the initial CV curve. It indicated that N doping could promote the formation of a carbon shell, which is crucial for enhancing its stability. The results demonstrated the promising potential of FeCo@CN-J-5 for seawater electrolysis applications.

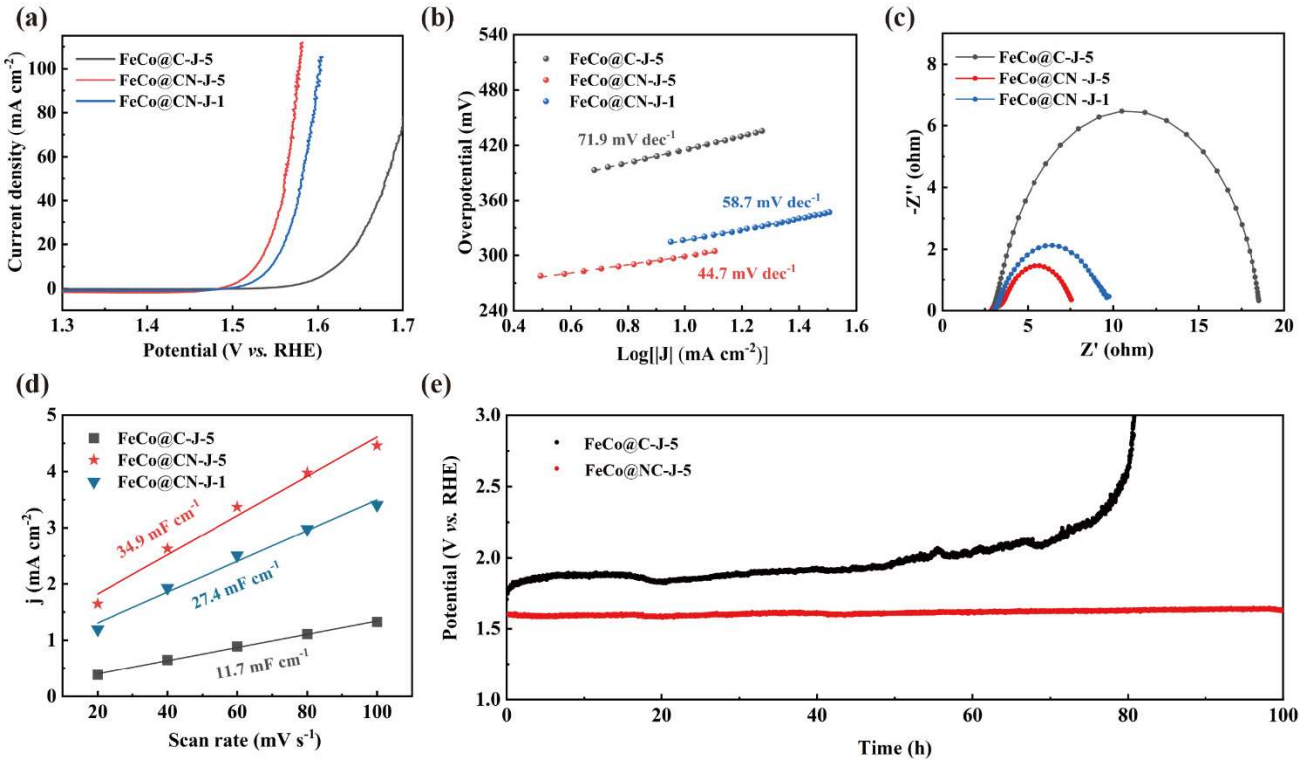

Figure 3. OER activity in weakly alkaline seawater. (a) CV curves in 0.1 M KOH + 0.6 M NaCl. (b) Tafel slope in 0.1 M KOH + 0.6 M NaCl. (c) EIS in 0.1 M KOH + 0.6 M NaCl at the potential of 1.56 V (vs. RHE). (d) C_{dl} and ECSA in 0.1 M KOH + 0.6 M NaCl. (e) Stability measurement of FeCo@C-J-5 and FeCo@CN-J-5 at the current density of 200 mA cm^{-2} in 0.1 M KOH + 0.6 M NaCl.

Structural stability evaluation

We further performed XRD, ICP, TEM, and XPS analyses to evaluate the chemical and structural stability differences before and after the OER stability test of FeCo@CN-J-5 (Figures 4a-4e). After the long-term OER test, the XRD pattern of FeCo@CN-J-5-After retained its characteristic peaks, indicative of its unchanged physical phase (Figure 4b and Figure S13). Meanwhile, the ICP results showed that the content of FeCo species in FeCo@CN-J-5-After slightly decreased and remained twice as high as that in FeCo@C-J-5-After (Table S2). Besides, in the TEM images (Figure 4a and Figure S14), unlike FeCo@C-J-5-After that experienced significant structure damage, FeCo@CN-J-5-After showed little change in its morphology after 100 h of stability testing. It demonstrated that the N-doped amorphous carbon shell had excellent encapsulation properties, effectively protecting the FeCo metal particles from being eroded by Cl^- in the solution.

The surface state was investigated using XPS, and the surface contents of Co, Fe, and N elements obtained from the XPS survey spectra (Figure S15 and Figure S16) were listed in Table S4. In contrast to FeCo@C-J-5 (Table S3), where the contents of Co and Fe decreased by approximately 30%, those in FeCo@CN-J-5-After almost unchanged, indicating that the N-doped carbon shell could effectively protect the FeCo metal nanoparticles. The collected spectra in Figures 4c-4e confirmed the survival of Fe, Co, and N species during long-term seawater oxidation stability test. For N 1s spectrum, there was a decrease in the amount of pyridine N and an increase in porphyrin-like metal N-coordinated M-N_x (Figure 4c), suggesting the capture of more Fe/Co atoms by N anchoring sites. Meanwhile, the Co 2p and Fe 2p spectra verified the increased of Co^{3+} and Fe^{3+} proportions, which were more favorable for charge transfer, thereby enhancing the reactivity of the catalyst (Figure 4d-f). To summarize, FeCo@C-J-5 was unable to form a stable carbon shell due to the lack of N elements, resulting in poor stability. In contrast, the unique properties of FeCo@CN-J-5, including the N-doped carbon shell and the dispersion of metal particles within the shell, endowed the catalyst with long-term stability.

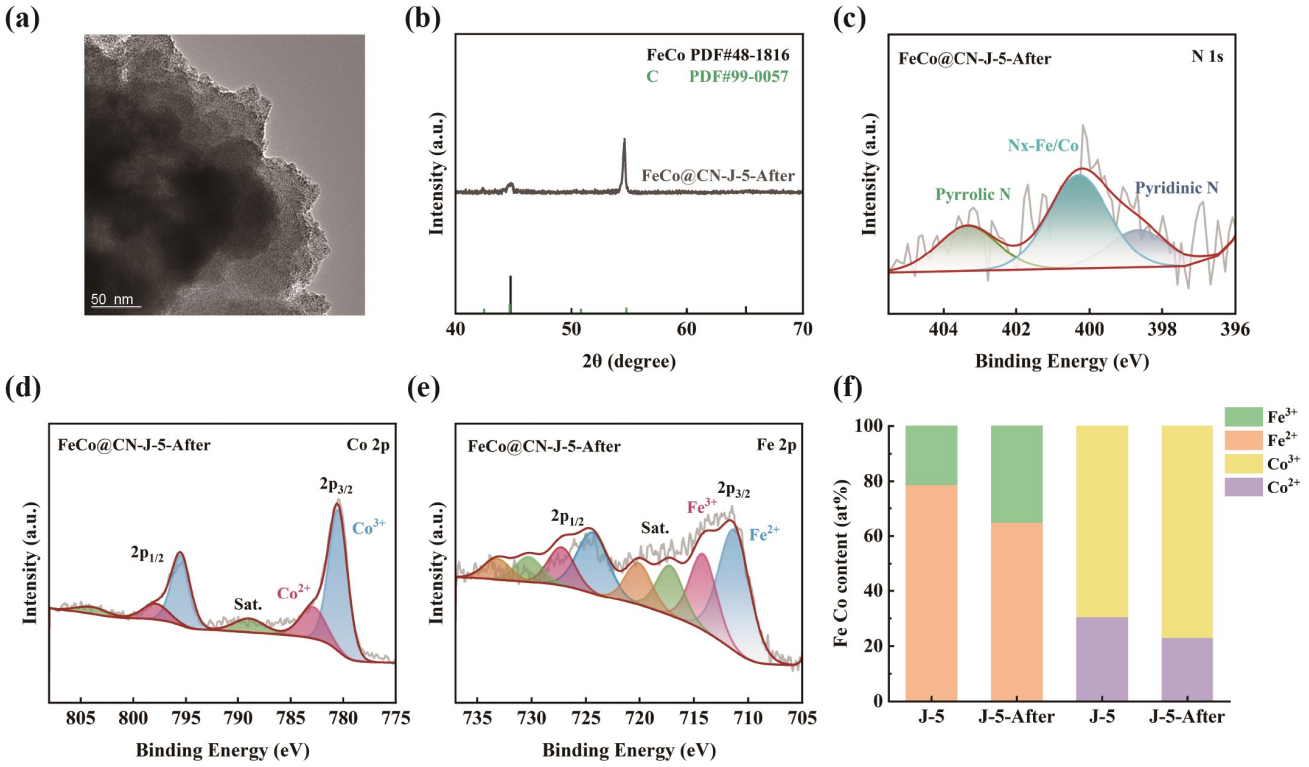

Figure 4. Stability and morphological and structural characterization. (a) The TEM images of FeCo@CN-J-5-After. (b) The XRD pattern of FeCo@CN-J-5-After. (c-e) XPS spectra of FeCo@CN-J-5-After. (f) Comparison of Fe and Co contents of FeCo@CN-J-5 and FeCo@CN-J-5-After.

Carbon shell encapsulation control

To further verify the critical requirement of rapid Joule-heat input for the encapsulation of FeCo metal nanoparticle and the full dispersion of Fe/Co-N_x-C active sites on the carbon shell, FeCo@CN-T-800-2 sample was synthesized by conventional heat treatment in a tube furnace using the same carbon paper substrate and Fe/Co/N precursors. The OER performance of FeCo@CN-T-800-2 was also evaluated using a three-electrode system in 0.1 M KOH+0.6 M NaCl solution. As shown in Figure 5a, FeCo@CN-T-800-2 required a higher overpotential (336 mV) at a current density of 10 mA cm^{-2} compared to FeCo@CN-J-5 (299 mV), indicating inferior OER performance. Meanwhile, at the overpotential of 350 mV, the current density of FeCo@CN-J-5 (125 mA cm^{-2}) was 6 times that of FeCo@C-J-5 (21 mA cm^{-2}). Figure 5b showed the long-term stability tests of FeCo@CN-T-800-2 and

FeCo@CN-J-5 at the current density of 200 mA cm^{-2}. It could be seen that FeCo@CN-T-800-2 decayed constantly, and completely lost its activity after 60 h, while FeCo@CN-J-5 operated much more stably over 100 hours.

XRD and XPS spectra showed that the crystal structure and surface chemical state of FeCo@CN-T-800-2 were consistent with that of FeCo@CN-J-5, as both samples were synthesized by heating in an argon atmosphere (Figure 5d-f and Figure S17-18). However, due to the slow heating rate and long heating duration of the conventional furnace heating, the metal species of FeCo@CN-T-800-2 aggregated into large nanoparticles (several hundred nanometers), and were encapsulated by an uneven carbon shell, whose thickness could be as low as 6.3 nm (Figure 5c and Figure S19). Meanwhile, the XPS results demonstrated that the carbon shell of FeCo@CN-T-800-2 contained much fewer Fe and Co atoms, leading to its reduction of active sites and OER activity (Table S3). Consequently, the OER performance of FeCo@CN-T-800-2 was not as good as that of FeCo@CN-J-5, and the carbon shell was too thin to protect the FeCo metal core from the corrosion of Cl^- in the stability test.

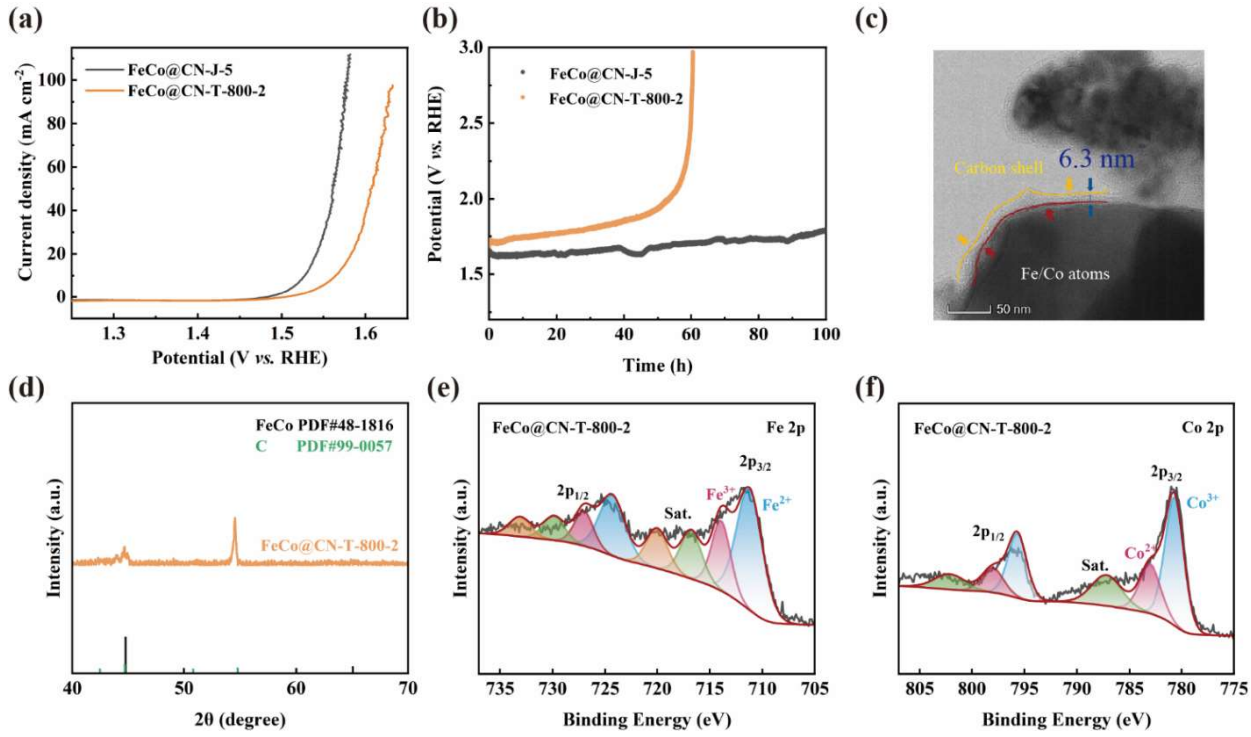

Figure 5. Comparison of the catalysts prepared by different heat treatment processes. (a) CV curves in 0.1 M KOH + 0.6 M NaCl. (b) Stability measurement of FeCo@CN-J-5 and FeCo@CN-T-

800-2 at the current density of 200 mA cm^{-2} in 0.1 M KOH + 0.6 M NaCl . (c) TEM images of FeCo@CN-T-800-2. (d) The XRD pattern of FeCo@CN-T-800-2. (e-f) XPS spectra of FeCo@CN-T-800-2.

Conclusions

The FeCo@CN-J-5 catalyst, featuring FeCo metal cores encapsulated in N-doped carbon shells, was prepared by the transient Joule heating method in several seconds. The high temperature (~800 ºC) could offer sufficient activation energy for Co/Fe atom redispersion on the carbon shell via forming the Co/Fe-N-C active sites. And the proper extension of the heating time led to the full redispersion of Fe/Co atoms in the N-doped carbon shell. The structure endowed FeCo@CN-J-5 with excellent OER performance, characterized by a low overpotential (299 mV at 10 mA cm^{-2}), a small Tafel slope (44.7 mV dec^{-1}), and outstanding long-term stability, as it maintained stable catalytic activity at a current density of 200 mA cm^{-2} for 100 hours.

Supporting Information

Supporting Information is available from the Wiley Online Library or from the author.

Acknowledgements

The authors gratefully acknowledge the research funding provided by National Key R&D Program of China (Grant No. 2021YFB3801301), National Natural Science Foundation of China (Grant Nos. 22378119, 22075076, and 22208092), and Shanghai Pilot Program for Basic Research (22TQ1400100-4).

Conflicts of Interest

The authors declare that they have no known competing financial interests or personal relationships that could have appeared to influence the work reported in this paper.

Data Availability Statement

The data that support the findings of this study are available from the corresponding author upon reasonable request.

Received: ((will be filled in by the editorial staff))
Revised: ((will be filled in by the editorial staff))
Published online: ((will be filled in by the editorial staff))

References

1 W. Li, J. Yang, D. Wang, *Angew. Chem. Int. Ed.* **2022**, *61*, e202213318.

2 H. Melin, *Nat. Astron* **2020**, *4*, 837.

3 N. Sazali, *Int. J. Hydrog. Energy* **2020**, *45*, 18753.

4 X. Yang, J. Cheng, X. Yang, Y. Xu, W. Sun, J. Zhou, *Chem. Eng. J.* **2023**, *451*, 138977.

5 P. Shen, B. Zhou, Z. Chen, W. Xiao, Y. Fu, J. Wan, Z. Wu, L. Wang, *Appl Catal B-Environ* **2023**, *325*, 122305.

6 L. Qi, J. Guan, *Green Energy Environ.* **2024**, DOI: 10.1016/j.gee.2024.07.009.

7 X. Wang, H. Zhong, S. Xi, W. S. V. Lee, J. Xue, *Adv. Mater.* **2022**, *34*, 2107956.

8 P. Kumar, K. Kannimuthu, A. S. Zeraati, S. Roy, X. Wang, X. Wang, S. Samanta, K. A. Miller, M. Molina, D. Trivedi, J. Abed, M. A. Campos Mata, H. Al-Mahayni, J. Baltrusaitis, G. Shimizu, Y. A. Wu, A. Seifitokaldani, E. H. Sargent, P. M. Ajayan, J. Hu, M. G. Kibria, *J. Am. Chem. Soc.* **2023**, *145*, 8052.

9 Z. Guan, J. Li, S. Li, K. Wang, L. Lei, Y. Wang, L. Zhuang, Z. Xu, *Mater. Chem. Front.* **2024**, *8*, 824.

10 L. Xiao, Z. Wang, J. Guan, *Chem. Sci.* **2023**, *14*, 12850.

11 J. Li, F. Xu, K. Wang, J. He, Y. Wang, L. Lei, M. Zhu, L. Zhuang, Z. Xu, *Chem. Eng. Sci.* **2023**, *267*, 118366.

12 S. Dresp, F. Dionigi, M. Klingenhof, P. Strasser, *ACS Energy Lett.* **2019**, *4*, 933.

13 C. Das, P. Roy, *Chem. Commun.* **2022**, *58*, 6761.

14 J. Ding, H. Yang, H. Zhang, Z. Wang, Q. Liu, L. Feng, G. Hu, J. Luo, X. Liu, *Int. J. Hydrog. Energy* **2024**, *53*, 318.

15 Z. Lu, H. Yang, G. Qi, Q. Liu, L. Feng, H. Zhang, J. Luo, X. Liu, *Small* **2024**, *20*, 2308841.

16 T. Tang, X. Bai, X. Xu, Z. Wang, J. Guan, *J. Colloid Interface Sci.* **2025**, *680*, 676.

17 L. Yu, Q. Zhu, S. Song, B. McElhenny, D. Wang, C. Wu, Z. Qin, J. Bao, Y. Yu, S. Chen, Z. Ren, *Nat. Commun.* **2019**, *10*, 5106.

18 L. Zhang, J. Liang, L. Yue, K. Dong, J. Li, D. Zhao, Z. Li, S. Sun, Y. Luo, Q. Liu, G. Cui, A. Ali Alshehri, X. Guo, X. Sun, *Nano Res. Energy* **2022**, *1*, 9120028.

19 F. Zhang, L. Yu, L. Wu, D. Luo, Z. Ren, *Trends Chem.* **2021**, *3*, 485.

20 J. Ding, Z. Peng, Z. Wang, C. Zeng, Y. Feng, M. Yang, G. Hu, J. Luo, X. Liu, *J. Mater. Chem. A* **2024**, *12*, 28023.

21 L. Yu, J. Xiao, C. Huang, J. Zhou, M. Qiu, Y. Yu, Z. Ren, C.-W. Chu, J. C. Yu, *Proc. Natl. Acad. Sci. U.S.A.* **2022**, *119*, e2202382119.

22 D. Zhang, H. Cheng, X. Hao, Q. Sun, T. Zhang, X. Xu, Z. Ma, T. Yang, J. Ding, X. Liu, M. Yang, X. Huang, *ACS Catal.* **2023**, *13*, 15581.

23 H. J. Song, H. Yoon, B. Ju, D.-Y. Lee, D.-W. Kim, *ACS Catal.* **2020**, *10*, 702.

24 L. Bigiani, D. Barreca, A. Gasparotto, T. Andreu, J. Verbeeck, C. Sada, E. Modin, O. I. Lebedev, J. R. Morante, C. Maccato, *Appl Catal B-Environ* **2021**, *284*, 119684.

25 Y. Kuang, M. J. Kenney, Y. Meng, W.-H. Hung, Y. Liu, J. E. Huang, R. Prasanna, P. Li, Y. Li, L. Wang, M.-C. Lin, M. D. McGehee, X. Sun, H. Dai, *Proc. Natl. Acad. Sci. U.S.A.* **2019**, *116*, 6624.

26 S. Loomba, M. W. Khan, M. Haris, S. M. Mousavi, A. Zavabeti, K. Xu, A. Tadich, L. Thomsen, C. F. McConville, Y. Li, S. Walia, N. Mahmood, *Small* **2023**, *19*, 2207310.

27 Z. Gong, J. Liu, M. Yan, H. Gong, G. Ye, H. Fei, *ACS Nano* **2023**, *17*, 18372.

28 Z. Su, C. Zhang, J. Liu, C. Liang, *J. Electroanal. Chem.* **2024**, *960*, 118182.

29 Y. Lei, F. Zhang, G. Li, J. Yang, H. Hu, Y. Shen, X. Zhang, X. Wang, *Int. J. Hydrog. Energy* **2024**, *65*, 437.

30 X. Lin, L. Cui, X. Ding, Y. Chen, Q. Wei, B. Huang, Z. Xie, *J. Alloy Compd.* **2024**, 174805.

31 J. Han, J. Sun, S. Chen, S. Zhang, L. Qi, A. Husile, J. Guan, *Adv. Mater.* **2024**, *36*, 2408139.

32 T. Tang, J. Han, Z. Wang, X. Niu, J. Guan, *Nano Res.* **2024**, *17*, 3794.

33 W. Ju, A. Bagger, G.-P. Hao, A. S. Varela, I. Sinev, V. Bon, B. Roldan Cuenya, S. Kaskel, J. Rossmeisl, P. Strasser, *Nat. Commun.* **2017**, *8*, 944.

34 D. Guo, R. Shibuya, C. Akiba, S. Saji, T. Kondo, J. Nakamura, *Science* **2016**, *351*, 361.

35 Y. He, H. Guo, S. Hwang, X. Yang, Z. He, J. Braaten, S. Karakalos, W. Shan, M. Wang, H. Zhou, Z. Feng, K. L. More, G. Wang, D. Su, D. A. Cullen, L. Fei, S. Litster, G. Wu, *Adv. Mater.* **2020**, *32*, 2003577.

36 C.-W. Liao, S.-Y. Chen, L.-C. Hsu, C.-W. Lin, J.-L. Chen, C.-H. Kuo, Y.-H. Chang, *ACS Sustainable Chem. Eng.* **2022**, *10*, 431.

37 Y. Yao, Z. Huang, P. Xie, L. Wu, L. Ma, T. Li, Z. Pang, M. Jiao, Z. Liang, J. Gao, Y. He, D. J. Kline, M. R. Zachariah, C. Wang, J. Lu, T. Wu, T. Li, C. Wang, R. Shahbazian-Yassar, L. Hu, *Nat. Nanotechnol.* **2019**, *14*, 851.